Proceedings of the 7th International Conference on HydroScience and Engineering

Philadelphia, USA September 10-13, 2006 (ICHE 2006)

ISBN: 0977447405

Drexel University

College of Engineering

ALTERNATING BARS IN TRANSCRITICAL FLOWS

Andrés Tejada-Martínez[1] and Cesar Mendoza[2]

ABSTRACT

A theoretical analysis is conducted to study qualitatively the development of alternate bars as the flow transitions from low- to high-Froude numbers. The model formulation adopted is that of Schielen et al. (1993), excluding their rigid-lid approximation for the flow free-surface and re-expressed in terms of local water depth, leading to the appearance of the Froude number in the dimensionless flow and sediment transport equations. For width-to-depth ratios above a minimum value, the alternate bars are influenced by the width of the channel; below this value, solutions to the model do not exist as such values of width-to-depth ratios correspond to the small-scale bed–wave regime. However, once the width-to-depth ratio is in the large-scale bed-wave regime, the Froude number plays an important role in separating stable and unstable regions. The quasi-steady nature of the flow model does not support the formation of neither stationary nor migrating *alternate antibars* (alternate bars that migrate upstream). It was found that the model can yield alternate bars under trans-critical and supercritical flow conditions, such as those in the laboratory observations of Ikeda (1984). When the width-to-depth ratio is greater, but still close to the minimum value required for the alternate bars to exist, low-Froude number instability does not occur as the bars only appear at sufficiently high Froude numbers. Low-Froude number instability takes place when the width-to-depth ratio increases past a certain amount above the minimum value required for the existence of the bars. In addition, the region of instability grows in size with higher width-to-depth ratios.

1. INTRODUCTION

Alternate bars occur in approximately straight reaches of natural or field-size shallow streams. They are distributed periodically along the stream reach, with consecutive bars on opposite sides of the channel. The study of this rhythmic bed pattern has been motivated by the plain beauty and regularity of the phenomenon, the destabilization of the channels in which they emerge and the associated side bank erosion, obstruction in navigation channels, and their possible connection to the initiation of stream meandering.

The emergence of alternate bars from an erodible bed has been treated as a problem of instability of the flow-bed boundary. Following this line of inquiry, linear theories were proposed by Fredsøe (1978), Blondeaux and Seminara (1985), Colombini et al. (1987), Nelson (1990), Schielen et al. (1993), Lanzoni and Tubino (1999) and most recently by Hall (2004). The weakly-nonlinear

[1] Assistant Professor, Department of Civil and Environmental Engineering, University of South Florida, Tampa, FL 33620, USA (tejada@ccpo.odu.edu)
[2] Associate Professor, Department of Civil, Architectural & Environmental Engineering, University of Missouri-Rolla, Rolla, MO 65409, USA (mendozac@umr.edu)

evolution of alternate bars has been studied by Fukuoka et al. (1985), Colombini et al. (1987), and Schielen et al. (1993).

Although an examination of laboratory experimental data on formed alternate bars (e.g. Ikeda 1984) reveals their existence at near-critical and supercritical flow conditions, existing theories on alternate bar formation have paid little attention to their their development as the flow transitions from low to high Froude numbers. Freeboard requirements for natural and man-made channel reaches with beds covered with alternate bars subjected to transcritical/supercritical regime flow conditions during floods makes it necessary to investigate the interaction of the stream and the bed formations under these flow conditions.

In this investigation, the alternate bars model proposed by Schielen et al. (1993) (hereafter SDdS), excluding their rigid-lid approximation for the flow free-surface, is used as the base for performing a linear stability analysis to explore qualitatively the behaviour of alternate bars under trans-critical and supercritical flow conditions.

2. GOVERNING EQUATIONS

The stream bed-flow interaction is modeled with equations governing the depth-averaged shallow water flow coupled with a bed evolution equation. The stream channel is taken to be straight, the banks vertical and non-erodible, and the stream bed made of non-cohesive material. The use of the depth-averaged shallow water flow is justified when considering the typical large width-to-depth ratio, $R=B/H$, for this phenomenon (see Figure 1); B and H are the width (i.e. the distance between the banks) and the unperturbed depth of the channel, respectively. A right-handed coordinate system is arranged so that x is the streamwise direction (aligned with the flow), y is the horizontal direction perpendicular to the flow and the banks, and z is the vertical direction. The dimensional model equations are

$$\frac{\partial \mathbf{u_h}}{\partial t} + \left(\mathbf{u_h}\cdot\nabla\right)\mathbf{u_h} + g\nabla\left(h+z_b\right) = \mathbf{G} \tag{1}$$

$$\frac{\partial h}{\partial t} + \nabla\cdot\left(\mathbf{u_h}\, h\right) = 0$$

$$\frac{\partial z_b}{\partial t} + \nabla\cdot\mathbf{q} = 0$$

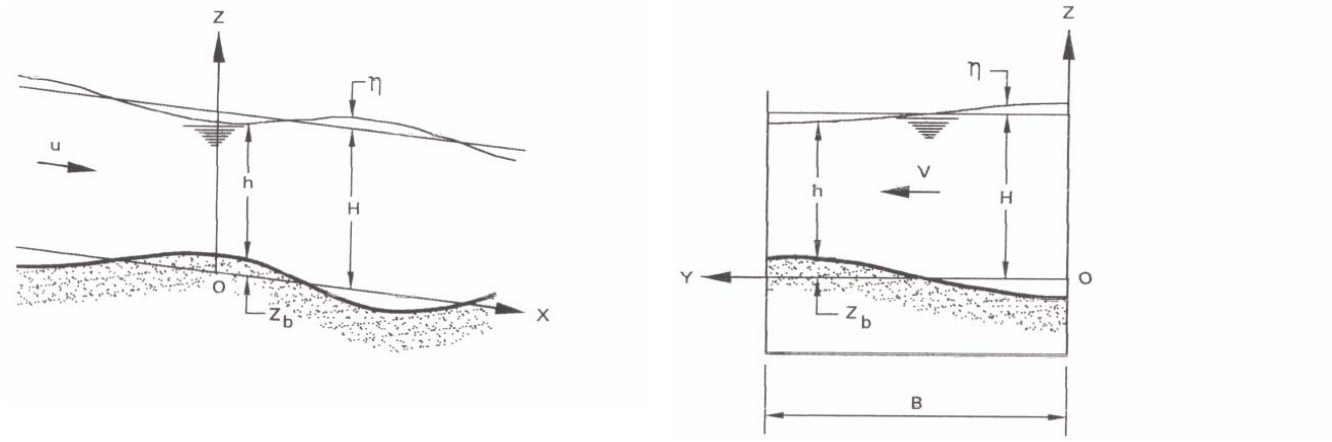

Figure 1 Sketch of coordinate system and variables.

where $\mathbf{u_h} = (u, v, 0)$ is the depth-averaged velocity vector in the *x*-*y* horizontal plane, *u* is the velocity in the *x*-direction, v is the velocity in the y-direction, z_b is the elevation of the perturbed bed relative to the original bed level, and h is the local water depth. The reader is directed to Figure 1 for a sketch of the coordinate system and variables.

The vector **G** representing forcing due to the channel slope and friction is taken as

$$\mathbf{G}=\left(i_o g - Cu\frac{|\mathbf{u_h}|}{h},\ -Cv\frac{|\mathbf{u_h}|}{h}\right) \tag{2}$$

where $C=g/C_f^2$ is a drag coefficient, *g* is gravity, i_o is the channel uniform slope, and C_f is the Chézy coefficient. Hence, the bottom stress is modelled in the direction of the depth-averaged velocity. The volumetric sediment flux, **q**, is given by the empirical formula:

$$\mathbf{q}=\sigma|\mathbf{u_h}|^b\left(\frac{\mathbf{u_h}}{|\mathbf{u_h}|}-\gamma\nabla z_b\right)=(q_x, q_y) \tag{3}$$

where *b* and σ are positive constants that depend on the bed porosity and sediment properties. As in SDdS, the constant γ is *O(1)*, therefore taken as $\gamma=1$ from the onset. It is assumed that the functional form of eq. 3 remains valid to model the volumetric bed load transport under trans-critical and supercritical flow conditions.

The system formed by eqs. 1, 2 and 3 can be closed by applying the following boundary conditions at the walls of the channel:

$$v(t,x,0)=v(t,x,L)=q_x(t,x,L)=q_y(t,x,L)=0. \tag{4}$$

The variables are made non-dimensional by making the following substitutions into the model:

$$\begin{aligned}\mathbf{x}=(x,y)&=(Lx', Ly'),\quad z_b=(U^2/g)z_b',\quad h=(U^2/g)h',\\ \mathbf{u_h}=(u,v,0)&=(Uu',Uv',0),\quad t=Tt'=(LU^{2-b}/g\sigma)t',\end{aligned} \tag{5}$$

where *L* is the channel width, and *U* is the magnitude of the characteristic flow velocity in its unperturbed state. Note that the previous assumption of a constant velocity profile introduces a fictitious slip velocity at the walls of the channel; however, this slip velocity does not play a role in the analysis because the banks are taken as non-erodible. The scaling for z_b and h was chosen such that there is a balance between advection terms and the pressure gradient. Because the focus of the analysis is on the instability of the bed, the time scale T is determined by the evolution of the bed. Assuming $L/UT << 1$ (implying that the flow is quasi-steady and instantaneously adapts to the evolution of the bed) and dropping primes for ease of notation, the system becomes:

$$\begin{aligned}\left(\mathbf{u_h}\cdot\nabla\right)\mathbf{u_h}+\ g\nabla\left(h+z_b\right)\ &=\ \mathbf{G}\\ \nabla\cdot\left(\mathbf{u_h}h\right)\ &=\ 0\\ \frac{\partial z_b}{\partial t}\ +\ \nabla\cdot\mathbf{q}\ &=\ 0\end{aligned} \tag{6}$$

where

$$\mathbf{G} = CR\left(1 - u\frac{|\mathbf{u_h}|}{F^2 h},\ -C\,v\frac{|\mathbf{u_h}|}{F^2 h}\right) \tag{7}$$

and

$$\mathbf{q} = |\mathbf{u_h}|^b\left(\frac{\mathbf{u_h}}{|\mathbf{u_h}|} - \frac{F^2}{R}\nabla z_b\right) \tag{8}$$

The previous expression was obtained by using $i_o/C = F^2$, thereby imposing a balance between forcing and dissipatio. The dimensionless model equations are closed by the boundary conditions in eq. 4, except that now the channel walls are located at $y=0$ and $y=1$.

From eqs. 6-8, the basic state of the dimensionless model is expressed as

$$\mathbf{s_o} = (u_o, v_o, h_o, z_{b\mathbf{o}}) = (1, 0, F^{-2}, 0). \tag{9}$$

In the next section, a perturbation of this basic state will be considered in order to study the stability of the state. Note that if the Froude number is retained in the model studied by SDdS, it becomes equivalent to the model studied here in eqs 6-8. However, the SDdS model is expressed in terms of variables $\mathbf{u_h}$, z_b and η (the deviation of the free surface away from its unperturbed level in Figure 1), which together with the scaling used, yields a sediment flux vector that does not include the Froude number, *F*. The model here has been expressed with the variable *h* instead of η to capture the influence of the Froude number on the dimensionless sediment flux vector. It can be seen in eq. 8 that the proportionality of the sediment of flux on the sand bed gradient is in terms of *F*; this is consistent with setting $i_o/C = F^2$ (i.e. the bed slope and *F* are proportional to each other in the unperturbed state). It is expected the Froude number to play an important role in the stability of the bed as it appears in both, the flow equations and the sediment transport equation.

3. LINEAR STABILITY ANALYSIS

The basic state in eq. 9 is perturbed in such a way that the new state is $\mathbf{s} = \mathbf{s_o} + \mathbf{s}'$ or

$$(u, v, h, z_b) = (u_o, v_o, h_o, z_{b\mathbf{o}}) + (u', v', h', z_b') \tag{10}$$

where the primed variables are small perturbations. Inserting this solution into the system formed by eqs. 6-8 and neglecting nonlinear terms, four partial differential equations governing the perturbations can be found. After dropping primes for ease of notation, these four equations can be represented in matrix form as

$$\mathbf{K}\,\mathbf{s}^t = \mathbf{0} \tag{11}$$

where $\mathbf{s}^t$ is the transpose of the solution vector $\mathbf{s}$ and matrix $\mathbf{K}$ is

$$\mathbf{K} = \begin{bmatrix} \partial_x + 2CR & 0 & \partial_x - CRF^2 & \partial_x \\ 0 & \partial_x + CR & \partial_y & \partial_y \\ \partial_x & \partial_y & F^2\partial_x & 0 \\ b\partial_x & \partial_y & 0 & \partial_t - (F^2/R)\nabla^2 \end{bmatrix} \tag{12}$$

The channel geometry allows for the decomposition of the perturbation vector as a traveling wave multiplied by an unknown lateral structure. Thus, an appropriate solution is of the form

$$\mathbf{s} = \mathbf{f}(y)e^{i(kx-\omega t)} + c.c. \;=\; \mathbf{f}(y)e^{-\omega_r t}\, e^{i(kx-\omega t)} + c.c. \tag{13}$$

where k is a real-valued, dimensionless wave number, ω is the complex, dimensionless frequency, and *c.c.* denotes the complex conjugate of the preceding term. Homogeneous boundary conditions at the banks allow for an oscillating solution in the y-direction. Thus, by inspecting the structure of the matrix $\mathbf{K}$, the vector function $\mathbf{f}(y)$ is written as

$$\mathbf{f}(y) = (\alpha_u \sin(p\pi y),\ \alpha_v \sin(p\pi y),\ \alpha_h \sin(p\pi y),\ \alpha_{zb} \sin(p\pi y)) \quad \text{for} \quad p=1,2\ldots \tag{14}$$

thereby enabling **s** to satisfy the boundary conditions. Alternate bars correspond to the $p=1$ mode, however, other modes will be addressed in our discussion as well. Inserting the solution in eqs. 13 and 14 into eq. 11 results in a linear system with constants α_u, α_v, α_h, α_{zb}. Non-trivial solutions for these constants exist only if the determinant of the system is set to zero. Consequently, this solvability condition results in the following dispersion relation between ω and k for the case $p=1$, corresponding to alternate bars:

$$\omega = \frac{a_1 + ia_2}{a_3 + ia_4} = \omega_r + i\omega_i \tag{15}$$

where

$$a_1 = bF^2k^4 - CF^2k^4 + 4CF^4 + F^2k^2\pi^2 - 3CF^2k^2\pi^2 - 2CF^2\pi^4 \tag{16}$$

$$\begin{aligned} a_2 = {} & R^{-1}(F^4k^5 - F^2k^5 - 2F^2k^3\pi^2 + F^4k^3\pi^2 - F^2k\pi^4) \\ & - bCF^2k^3R - 3C^2F^4k^3R - 3CF^2k\pi^2R \\ & + bCF^2k\pi^2R - 3C^2F^4k\pi^2R \end{aligned} \tag{17}$$

$$a_3 = 4CF^2k^2R - Ck^2R - 2C\pi^2R \tag{18}$$

$$a_4 = F^2k^3 - k^3 - k\pi^2 - 3C^2F^2kR^2 \tag{19}$$

Using the dispersion relation in eq. 15 α_u, α_v, α_h, and α_{zb} can be determined up to a constant. The stability of the basic state is determined by ω_r, the real part of ω, as can be seen from eq. 13. If $\omega_r > 0$, perturbations will decay exponentially in time returning back to the basic state; in other words, the basic state is stable. However, if $\omega_r < 0$, then the basic state is unstable giving way to growing alternate bars in the case of $p=1$. The neutral curve in the *(k, F)*-plane which separates

the stable and unstable states can be obtained by setting $\omega_r = 0$. The curve $\omega_i = 0$ helps to distinguish between bed perturbations which migrate downstream, namely *alternate bars*, from those which migrate upstream, namely *alternate antibars*. If $\omega_i > 0$, alternate bars occur, and if $\omega_i < 0$, alternate antibars occur. The term *antibars* is analogous to the term *antidunes* commonly found in the literature. However, because this model considers a quasi-steady flow, it is unable to yield stationary or upstream migrating antibars; these two bed forms result from the interaction of surface gravity waves with the bottom. By imposing the quasi-steadiness, gravity waves are excluded from the depth-averaged shallow water equations and the only possibility for flow perturbations is to propagate with the same velocity as the bed perturbations. Thus, the present model yields only an instability region of the alternate bar type and not of the alternate antibar type. Typical values of *b, C, F*, and *k* were inserted into the expression for ω_i obtained from eq. 15 confirming that the present model only yields alternate bars. For a more detailed discussion of this the interested reader is directed to the article of Gradowczyk (1968).

4. RESULTS

Despite being written in different variables, the full model in eq.1 is equivalent to the model of SDdS. Consequently, the linear stability analysis of SDS is equivalent to the linear stability analysis presented here in the limit $F \to 0$. This is evinced in Figure 2 where the neutral stability curves associated with the linear stability analysis of eq. 1 in this limit together with the neutral curves obtained in the analysis of SDdS are depicted. The latter curve is defined as

$$\lambda = \frac{-X(X+1)^3\delta}{\delta(X+1)(X+2)^2 - X(2X+1)} \tag{20}$$

where

$$\lambda = \frac{C^2R^2}{p^2\pi^2}, \qquad X = \frac{k^2}{p^2\pi^2}, \qquad \delta = \frac{\gamma C}{\beta}, \qquad \beta = b-1. \tag{21}$$

Both curves are identical and thus the analysis of SDdS is a particular case of the more general linear stability analysis, valid for any *F*, presented here. An interesting note is that neutral curves only exist on the *(k, R)*-plane in the limit $F \to 0$. This suggests that the analysis of SDdS is only valid for the cases when *F<<1,* as they noted.

Neutral curves for finite values of *F* are shown in Figures 3 - 5. The range of parameters used to evaluate the neutral curves in Figures 3a - 5a was based on values suggested in SDdS, generally corresponding to the subcritical regime. The range of parameters used to evaluate the neutral curves in Figures 3b - 5b was based on experimental data reported by Ikeda (1984) for alternate bars existing in near-critical and supercritical flow conditions. Based on Ikeda's data, the range of values considered were $0.9<F<2.0$, $10<R<50$, $5<b<7$, $0.004<C<0.008$. For these parameters, typical alternate bar wavelengths were in the range $0.7<k<1.0$; this is consistent with the regions of instability resulting from the current linear stability analysis.

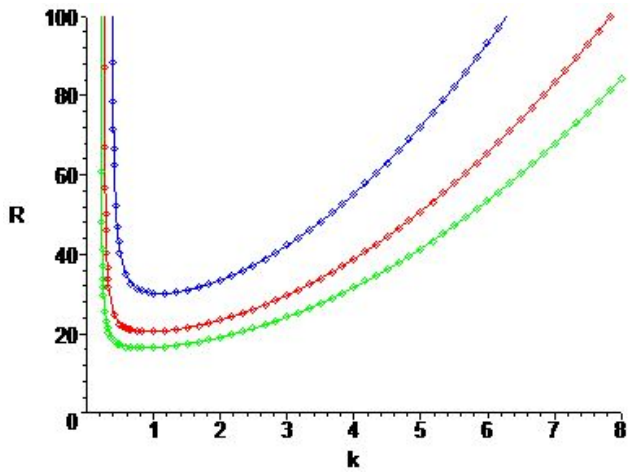

Figure 2 Neutral curves on (*k, R*)-plane obtained from current linear stability analysis in the limit $F \to 0$ and from eqs 20 and 21 of the model of SDdS (diamonds) for *b=3* (blue), *b=5* (green) and *b=7* (red). In all curves, *C=0.007*, *p=1* and $\gamma = 1$.

The neutral stability curves indicate that travelling wave solutions of the model linearized about its basic state exist for sufficiently large values of *R*. In addition, *F* also plays an important role in determining the stability of the basic state, as is evident in Figures 3 - 5. In the present analysis, for (*k, F*)-pairs lying inside the stability curves in Figures 3 - 5, the perturbation of the basic state is unstable and grows leading to alternate bars. For (*k, F*)-pairs lying outside of these curves, the perturbation decays leading to a flat bed. As can be observed from the examples in Figure 3, alternate bars can occur for both subcritical (*F<1*) and supercritical (*F>1*) regimes, depending on the value of *R*. For sufficiently small values of *R* (e.g. *R=24.87*), yet large enough for solutions of the model to exist, the bars occur only in the subcritical regime. In the examples of Figure 3a, when *F<<1*, instability and thus the formation of bars can occur if *R>24.9257*, suggesting that the analysis of SDdS would be valid only for such values of *R*.

Figure 3b shows additional neutral curves on the (*k, R*)-plane for values of *R* ranging from 30 to 90. These curves suggest a minimum value of the wave number (i.e. *k~0.3*) and a maximum value of the Froude number (i.e. *F~5.8*) at which bars can occur as *R* increases.

Figures 4 and 5 demonstrate the dependence of the instability region on parameters *b* and *C*, respectively. Similar to its dependence on *R*, the region of instability increases as *b* and *C* increase. Slight changes to *R*, *b* and *C* can result in great changes to the region of instability. For example, a slight perturbation of any these parameters can be the deciding factor in determining the stability of the basic state under low-Froude number conditions.

Finally, neutral curves such as those in Figures 3 - 5 (i.e. cases with $F \neq 0$) only exist for the *p=1* mode (i.e. the alternate bar mode). Thus, the alternate bar mode is the only mode that can become unstable. This is in contrast to the case in the limit $F \to 0$ for which higher modes can become unstable as well (see SDdS for further discussion).

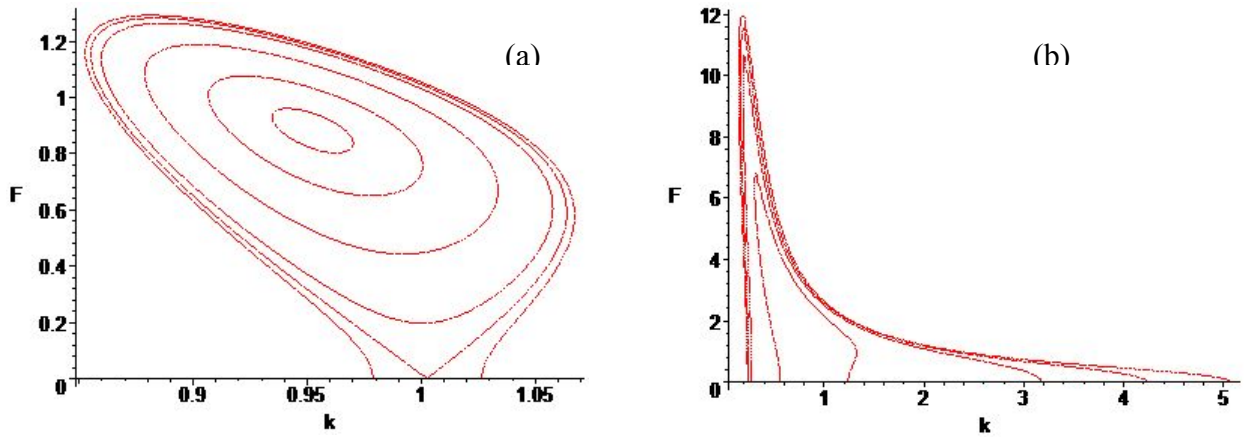

Figure 3 Neutral curves on the (*k, F*)-plane for various values of *R*. For the curves (a), *R=24.929*, *R=24.9257*, *R=24.92*, *R=24.88* and *R=24.87* with *C=0.007* and *b=3.8*. For the curves on (b), *R=20*, *R=30*, *R=40* and *R=50* with *C=0.006* and *b=6*. The instability region (inside the curves) grows as *R* increases.

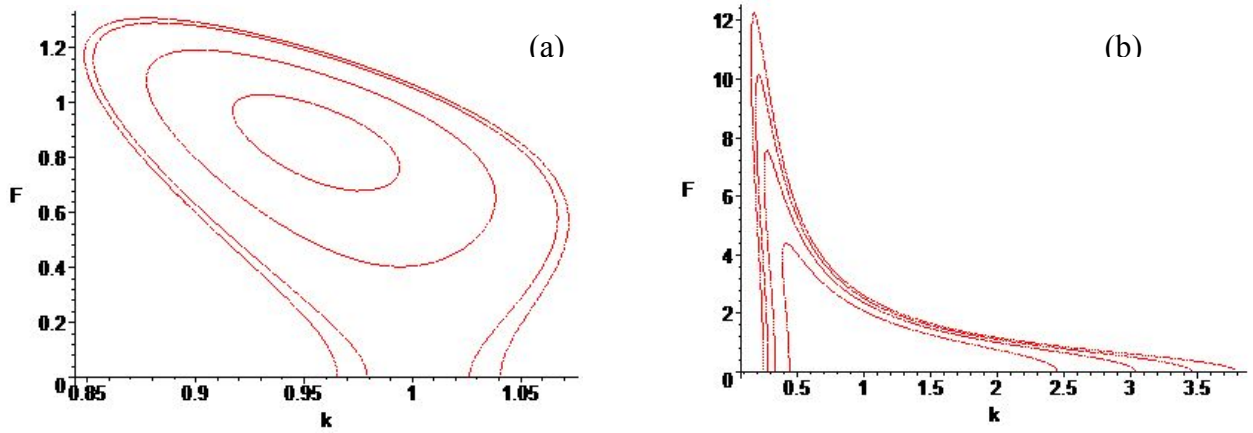

Figure 4 Neutral curves on the (*k, F*)-plane for various values of *b*. For the curves on (a), *b=3.79*, *b=3.795*, *b=3.8*, and *b=3.801* with *R=24.929* and *C=0.007*. For the curves on (b), *b=4*, *b=5*, *b=6* and *b=7* with *R=30* and *C=0.006*.

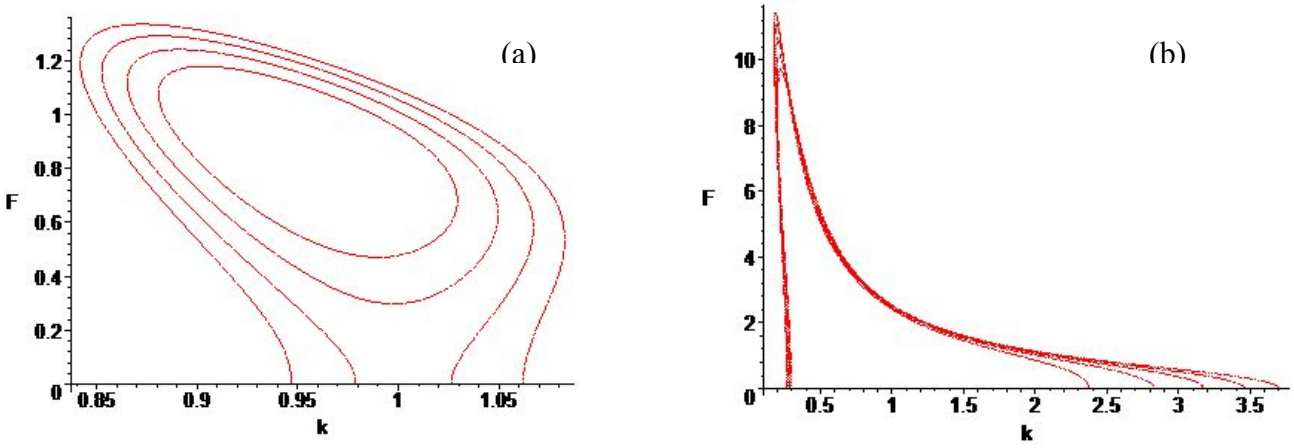

Figure 6 Neutral curves on the (*k, F*)-plane for various values of *C*. For the curves on (a), *C=0.00698, C=0.00699, C=0.007* and *C=0.00701* with *R=24.929* and *b=3.8*. For the curves on (b), *C=0.004, C=0.005, C=0.006, C=0.007* and *C=0.008* with *R=30* and *b=6*.

5. CONCLUSIONS

The results of the linear stability analysis based on the modified SDdS model indicate that both, the width-to-depth ratio *R* and the flow Froude number *F*, play important roles in determining the stability of the flow-bed boundary. Furthermore, results indicate that downstream-migrating alternate bars can occur in the transcritical and supercritical flow regimes. The model is unable to yield stationary and upstream-migrating alternate antibars. These results motivate future work toward the generalization of the weakly nonlinear analysis of SDdS for all valid *R* and for transcritical and supercritical values of *F*.

REFERENCES

Blondeaux, P. and Seminara, G. (1985) "A Unified Bar-Bend Theory of River Meanders," Journal of Fluid Mechanics, Vol.157, pp. 449-470.

Colombini, M., Seminara, G. and Tubino, M. (1987) "Finite-Amplitude Alternate Bars," Journal of Fluid Mechanics, Vol. 181, pp. 213-232.

Fredsøe, J. (1978) "Meandering and Braiding of Rivers," Journal of Fluid Mechanics, Vol. 84, Part 4, pp. 609-624.

Fukuoka, S. and Yamasaka, M. (1985) "Equilibrium Wave Height and Flow on Alternate Bar Based on Nonlinear Relationships of Bedform, Flow and Sediment Discharge," Proceedings 21st IAHR Congress, Melbourne, Australia, 19-23 August 1985.

Gradowczyk, M.H. (1968) "Wave Propagation and Boundary Instability in Erodible-Bed Channels", Journal of Fluid Mechanics, Vol. 33, Part 1, pp. 98-112.

Hall, P. (2004) "Alternating Bar Instabilities in Unsteady Channel Flows over Erodible Beds," Journal of Fluid Mechanics, Vol. 499, pp. 49-73.

Ikeda, S. (1984) "Prediction of Alternate Bar Wavelength and Height," Journal of Hydraulic Engineering, ASCE, Vol. 110, No. 4, pp. 371-386.

Lanzoni, S. and Tubino, M. (1999) "Grain Sorting and Bar Instability," Journal of Fluid Mechanics, Vol. 393, pp.149-174.

Nelson, J.M. (1990) "The Initial Instability and Finite-Amplitude Stability of Alternate Bars in Straight Channels," Earth Science Reviews, Vol. 29, Issues 1-4, pp. 97-115.

Schielen, R.S., Doelman, A. and de Swart, H.E. (1993) "On the Nonlinear Dynamics of Free Bars in Straight Channels", Journal of Fluid Mechanics, Vol. 252, pp. 325-356.